

This paper has been accepted for publication in the AEE journal. This is the version, which has not been fully edited and content may change prior to final publication.

Citation information: DOI 10.24425/ae.2025.153911

Cooperative optimization of temperature and thrust ripple in permanent magnet synchronous linear motors

JIANGLONG YAN¹, YANZHE LI^{1*}, YIMENG YANG², GUOQING LIU¹, YUANTAO LIU¹

¹*School of Automation and Electrical Engineer, Lanzhou Jiaotong University
NO.88, Anning West Road, Gansu Province, China*

²*Beijing Hollysys CO, LTD
Beijing Province, China*

*e-mail: {12231668/13240081/12211454}@stu.lzjtu.edu.cn, *yanzhe866@lzjtu.edu.cn,
yangyimeng1120@163.com*

Abstract: Temperature rise and thrust ripple in Permanent Magnet Synchronous Linear Motors are critical factors that impact their operational performance and stability. This study addresses the coupled effects of temperature variation and thrust ripple in Permanent Magnet Synchronous Linear Motors by proposing a cooperative optimization method aimed at enhancing stability and efficiency. A trapezoidal Halbach alternating electrode structure-based Permanent Magnet Synchronous Linear Motors analytical model was developed. Combining the Multi-Population Genetic Algorithm with the Kriging surrogate model, a cooperative optimization framework was established to improve the precision and efficiency of temperature and thrust ripple optimization through iterative sample point addition and multi-objective strategies. Experimental results demonstrate that the proposed method reduces thrust fluctuation to 8.3%, which is lower than traditional methods. The utilization rate of the permanent magnet is higher than other methods, reaching 5.8 N/cm³. The temperature rise is significantly reduced, achieving a maximum energy-saving rate of 25%, and the optimization efficiency improves by 43.5%. In addition, the reliability of the method is verified by COMSOL Multiphysics 6.0 finite element simulation combined with ANSYS Maxwell electromagnetic simulation. This research offers a novel approach to Permanent Magnet Synchronous Linear Motors optimization, providing technical insights for designing high-performance, energy-efficient motors.

Keywords: Permanent Magnet Synchronous Linear Motor, thrust ripple, temperature rise, Multi-Population Genetic Algorithm, Kriging

This paper has been accepted for publication in the AEE journal. This is the version, which has not been fully edited and content may change prior to final publication.

Citation information: DOI 10.24425/ae.2025.153911

Nomenclature

| Abbreviations | Full name |
|---------------|---|
| PMSLMs | Permanent Magnet Synchronous Linear Motors |
| GA | Genetic Algorithm |
| PSO | Particle Swarm Optimization |
| MPGA | Multi-Population Genetic Algorithm |
| THCP-PMSLM | Trapezoidal Halbach Cylindrical Permanent Magnet Synchronous Linear Machine |
| HCP-PMLSM | Halbach Configuration Primary Permanent Magnet Linear Synchronous Motor |
| DH-PMLSM | Double-layer Halbach Primary Permanent Magnet Linear Synchronous Motor |
| HSP-PMLSM | Heterogeneous Structure Primary Permanent Magnet Linear Synchronous Motor |
| MRP-PMLSM | Magnetic Reluctance-Optimized Primary Permanent Magnet Linear Synchronous Motor |
| VPP-PMLSM | Variable Pole Pitch Primary Permanent Magnet Linear Synchronous Motor |
| CCH-PMLSM | Composite Coil Halbach Primary Permanent Magnet Linear Synchronous Motor |
| DPSO | Differential Particle Swarm Optimization Algorithm |
| AMCO | Adaptive Multi-objective Cooperative Optimization Algorithm |

1. Introduction

With the advent of Industry 4.0, high-precision, high-efficiency motor drive systems have become essential components of modern industrial automation and intelligence [1–2]. Motors, as the core of power-driven devices, directly influence the operational efficiency and stability of the entire system [3–4]. Over decades, motor drive technologies have evolved rapidly, from traditional rotary motors to linear motors, which convert electrical energy directly into linear mechanical motion, bypassing the complex processes of gears and belts [5]. Linear motors offer advantages in energy efficiency, precision, and responsiveness, making them ideal for applications in rail transit, automated production lines, and precision instruments. Among linear motors, PMSLMs have emerged as a leading technology, widely used in industrial manufac-

This paper has been accepted for publication in the AEE journal. This is the version, which has not been fully edited and content may change prior to final publication.

Citation information: DOI 10.24425/ae.2025.153911

turing and rail transit [6]. However, practical applications often face challenges such as temperature rise and thrust ripple, which compromise motor stability and lifespan [7]. Recent studies on PMSLMs have introduced various structural designs and optimization methods, but significant limitations persist.

Many studies have attempted to improve the performance of the PMSLM by adjusting its electromagnetic design. Zhang Z. *et al.* suggested a technique to optimize the arrangement of permanent magnets based on the Halbach array. By altering the magnetization direction, this method reduces back leakage flux, effectively lowering thrust ripple and enhancing motor smoothness [8]. However, the problem of electromagnetic noise remains unresolved. Di J. *et al.* improved thrust performance significantly by altering the stator slot width, but the complex computational process of stator slot design limits the generalization ability of this method [9]. Yang X. *et al.* offered a strategy for optimizing the air-gap magnetic flux density distribution using the finite element method. By introducing a non-uniform magnetization distribution model in the air gap, thrust ripple was effectively reduced. However, this method does not consider the impact of temperature on performance [10]. Yun H. *et al.* proposed a combined optimization scheme for coil and magnetic pole structures. This method evaluated the thrust density improvement using electromagnetic simulation software, thereby enhancing the motor's thrust performance. However, the complex materials and manufacturing processes required make the method costly and difficult to widely adopt [11]. Chen Y. *et al.* explored an optimization method for asymmetric permanent magnet arrangements. By optimizing the spacing and shape of magnetic poles, thrust ripple was reduced. However, this method does not meet the precision and stability requirements of high-end industrial applications [12].

Collaborative optimization of thrust and temperature has also been a widely discussed topic in PMSLM research. Wu Y.Z. *et al.* presented an integrated optimization method based on surrogate models, establishing proxy models for thrust and temperature and using a GA to optimize the model settings. This method effectively achieved control of thrust and temperature but is challenging to apply in complex scenarios [13]. Zhang S. *et al.* proposed a collaborative optimization method for PMSLM temperature and thrust based on the PSO algorithm. This method balances thrust and stability through adaptive functions but is prone to local optima, making it difficult to obtain the global optimum solution [14]. Zhang S. *et al.* also proposed a thrust ripple improvement method based on the GA. By using crossover and mutation operations, thrust characteristics were optimized. However, this method requires a large amount of permanent magnet material, increasing motor manufacturing costs [15]. Huang M. *et al.* has been shown a motor temperature method based on the adaptive simulated

This paper has been accepted for publication in the AEE journal. This is the version, which has not been fully edited and content may change prior to final publication.

Citation information: DOI 10.24425/ae.2025.153911

annealing algorithm. By dynamically adjusting the temperature variation step size, the stability of the motor system was improved. However, the optimization process is time-consuming and cannot meet the demands for quick responses [16]. Mahmood D.Y. *et al.* demonstrated a collaborative method comprised of a multi-objective algorithm. By balancing the weights of temperature and thrust, motor performance was improved. However, this method relies heavily on initial parameters, making it challenging to ensure stability and accuracy in optimization results [17].

In summary, while the aforementioned methods have made progress in thrust and temperature optimization, they have limitations in convergence, reliability, and practical application efficiency. This research introduces a trapezoidal Halbach alternating pole structure and an MPGA to construct a THCP-PMSLM. Compared with the latest research, this study contributes by overcoming the limitations of the Halbach structure. It reduces thrust fluctuation while improving system adaptability. The proposed method uses an MPGA to address the local optimum issues of PSO and a GA, achieving a better balance between thrust and temperature optimization. Additionally, by integrating the Kriging surrogate model, this method enhances motor stability while considering cost-effectiveness and energy efficiency. The research is expected to provide a novel solution for PMSLM performance optimization in industrial scenarios, improving motor stability, adaptability, and cost-effectiveness, thereby offering theoretical and practical foundations for real-world applications.

2. Methods and materials

This study focuses on constructing an analytical model for PMSLMs based on the trapezoidal Halbach alternating electrode structure and developing an optimization framework.

2.1. Analytical model based on trapezoidal Halbach alternating electrode structure

PMSLMs are characterized by high thrust density, precision, and non-contact mechanical motion, making them indispensable in industrial automation and precision motion control [18]. However, thrust ripple reduces system stability and positional accuracy, while temperature rise may degrade material properties and exacerbate thermal mismatch, worsening thrust ripple [19–20]. The trapezoidal Halbach alternating electrode structure offers uniform magnetic field distribution and flux concentration, effectively reducing thrust ripple [21]. This section constructs an analytical model for the THCP-PMSLM. Therefore, based on the trapezoidal Hal-

This paper has been accepted for publication in the AEE journal. This is the version, which has not been fully edited and content may change prior to final publication.

Citation information: DOI 10.24425/ae.2025.153911

bach alternating electrode structure, this section constructs an analytical model of the THCP-PMSLM to quantify the relationship between temperature and thrust fluctuations, providing a theoretical basis for subsequent collaborative optimization. Firstly, Fourier decomposition method is used to quantify the magnetization distribution of Halbach structure, and an analytical expression for the air gap magnetic field is established, as shown in Eq. (1) [22].

$$B_g(x) = \sum_{n=1}^{\infty} B_n \cos(nkx). \quad (1)$$

In Eq. (1), $B_g(x)$ represents the air-gap magnetic flux density; B_n denotes the amplitude of the n -th harmonic of the magnetic flux density; k represents the wave number ($k = \frac{2\pi}{L}$, where L indicates the pole distance of the motor); x denotes the spatial position. Since thrust ripple directly affects the stability and accuracy of the motor, it is essential to quantify its magnitude and characteristics as a reference for optimization design. The calculation of thrust ripple characteristics is shown in Eq. (2).

$$F(t) = \int_0^L B_g(x) \cdot J(x) dx. \quad (2)$$

In Eq. (2), $F(t)$ represents the thrust; $J(x)$ represents the current density distribution. The coupling effect between electromagnetic force and volumetric force is a key factor affecting thrust stability. To clarify the comprehensive impact of this coupling on motor performance, the electromagnetic force and volumetric force are separately modeled to analyze their superimposed effects, as shown in Eq. (3).

$$F_{\text{total}} = F_{\text{em}} + F_{\text{vol}}. \quad (3)$$

In Eq. (3), F_{total} represents the total thrust; F_{em} represents the electromagnetic force; F_{vol} represents the volumetric force. The superimposed effects of electromagnetic force and volumetric force provide the basis for evaluating thrust density and efficiency performance. The analytical model for motor performance indicators is expressed in Eq. (4).

$$\eta = \frac{P_{\text{out}}}{P_{\text{in}}} = \frac{F \cdot v}{I \cdot V}. \quad (4)$$

In Eq. (4), η represents efficiency; P_{out} represents output power; P_{in} represents input power; F represents thrust; v represents speed; I represents current; V represents voltage. Since the

This paper has been accepted for publication in the AEE journal. This is the version, which has not been fully edited and content may change prior to final publication.

Citation information: DOI 10.24425/ae.2025.153911

pole pitch and magnet thickness significantly influence the magnetic field and thrust ripple, the optimization range of these parameters must be determined, as shown in Eq. (5).

$$P_k = \frac{\partial F}{\partial X_k} \cdot X_k. \quad (5)$$

In Eq. (5), P_k represents the parameter sensitivity coefficient; X_k represents the structural parameter. Based on the parameter ranges set above, the variation in motor performance under different parameter combinations is evaluated, as shown in Eq. (6).

$$R = \sqrt{\sum_{i=1}^n \left(\frac{F_i - \bar{F}}{\bar{F}} \right)^2}. \quad (6)$$

In Eq. (6), R represents the performance fluctuation rate; F_i represents the thrust in the i -th simulation; \bar{F} represents the average thrust. By optimizing the parameter ranges, the minimized thrust fluctuation amplitude and temperature amplitude are obtained and finally the best parameter combination is obtained to improve the motor performance. The expression of the optimization problem, as shown in Eq. (7).

$$\text{Opt} = \arg \min(w_1 \cdot \Delta F + w_2 \cdot \Delta T). \quad (7)$$

In Eq. (7), Opt represents the optimal parameter combination; ΔF represents the amplitude of thrust ripple; ΔT represents the amplitude of temperature fluctuation; w_1 and w_2 stand for the weight coefficients and are used to balance the relative importance of the two optimization objectives. When using Eq. (7) for the solution of the optimal parameters, if the function is differentiable, the optimal solution can be derived analytically; if the function is not derivable analytically, the optimal solution is obtained by the gradient descent method. The above steps provide a theoretical foundation for further motor optimization. The constructed analytical model for the THCP-PMSLM is illustrated in Fig. 1.

This paper has been accepted for publication in the AEE journal. This is the version, which has not been fully edited and content may change prior to final publication.

Citation information: DOI 10.24425/ae.2025.153911

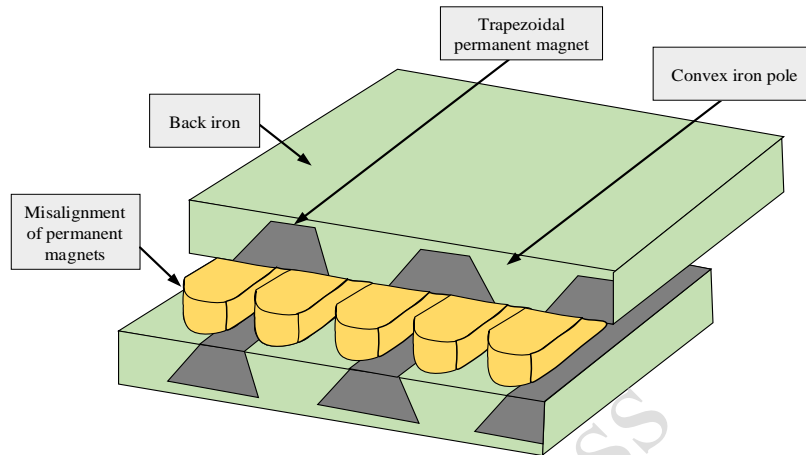


Fig. 1. Schematic diagram of THCP-PMSLM analytical model

Figure 1 shows a schematic diagram of the THCP-PMSLM analytical model, in which a trapezoidal Halbach array is distributed on the motor stator, utilizing its unique magnetic flux distribution characteristics to achieve efficient magnetic field utilization and low thrust fluctuation characteristics.

2.2. Coordinated optimization method of temperature and thrust ripple using MPGA and Kriging surrogate model

In the previous section, the effects of motor structural parameters on average thrust, thrust ripple, and thrust-to-volume ratio were preliminarily analyzed. However, due to the coupling relationships between the structural parameters in the analytical model, achieving optimization goals through simple parameter selection is challenging [23–24]. Furthermore, temperature rise and thrust ripple are crucial factors affecting motor performance and reliability [25–26]. Traditional optimization methods struggle to balance these two indicators effectively [27–28]. Therefore, this section introduces a new cooperative optimization strategy to balance motor temperature rise and thrust fluctuation. This strategy uses the Kriging surrogate model combined with MPGA. The specific optimization process is shown in Fig. 2.

This paper has been accepted for publication in the AEE journal. This is the version, which has not been fully edited and content may change prior to final publication.

Citation information: DOI 10.24425/ae.2025.153911

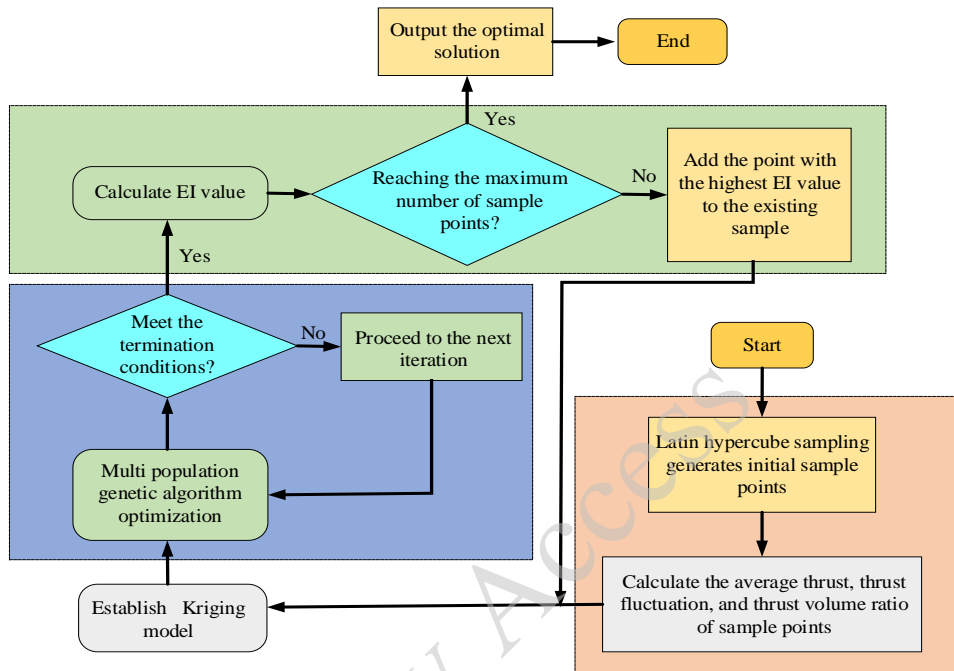


Fig. 2. Coordinated optimization flowchart

From Fig. 2, it can be observed that the strategy integrates the high-accuracy modeling capability of the Kriging surrogate model with the global optimization capability of MPGA. Additionally, it dynamically adds sample points using the Expected Improvement (EI) criterion to improve the prediction efficiency and accuracy of temperature rise and thrust ripple optimization. To construct the Kriging surrogate model, Latin Hypercube Sampling (LHS) is used to generate sample points, as shown in Eq. (8) [29].

$$X = \{(w_m^i, p^i, \theta_m^i)\}, \quad i = 1, 2, \dots, N. \quad (8)$$

In Eq. (8), X is the sample set of design variables; w_m^i represents the width of the permanent magnet at the i -th sample point; p^i indicates the polar distance of the i -th sample point; θ_m^i represents the inclination angle of the trapezoidal magnetic pole slope; N represents the amount of sample points. The generated sample points serve as the input data for constructing the Kriging surrogate model, which creates a nonlinear mapping that links the target response values and design variables, as shown in Eq. (9).

This paper has been accepted for publication in the AEE journal. This is the version, which has not been fully edited and content may change prior to final publication.

Citation information: DOI 10.24425/ae.2025.153911

$$y(X) = \mu + Z(X). \quad (9)$$

In Eq. (9), $y(X)$ is the target response value; μ is a constant baseline value; $Z(X)$ is a zero-mean Gaussian process representing random errors. In the optimization of the PMSLM, both temperature rise and thrust ripple need to be considered comprehensively [30–31]. For this multi-objective optimization problem, the objective function and weight allocation must be explicitly defined, as shown in Eq. (10).

$$f_{\text{obj}} = w_3 \cdot \Delta T(X) + w_4 \cdot \Delta F(X). \quad (10)$$

In Eq. (10), f_{obj} is the optimization objective function; $y_1(X)$, $y_2(X)$ and $y_3(X)$ all represent target response values; w_3 and w_4 represent the target weights, reflecting the relative importance of temperature rise and thrust fluctuations; $\Delta T(X)$ and $\Delta F(X)$ represent the function values of temperature rise and thrust fluctuation, respectively. Using the global search capability of MPGA, the temperature rise and thrust parameters in the objective function are preliminarily optimized, as shown in Eq. (11) [32].

$$\text{Fitness}(X) = f_{\text{obj}}(X). \quad (11)$$

In Eq. (11), $\text{Fitness}(X)$ represents the fitness value; $f_{\text{obj}}(X)$ is the objective value calculated by the surrogate model. Based on the preliminary optimization results, the accuracy of the surrogate model is improved by selecting new sample points using the EI criterion, as shown in Eq. (12).

$$\begin{cases} EI(X) = \sigma(X) \cdot [Z \cdot \Phi(Z) + \phi(Z)] \\ Z = \frac{\hat{y}(X) - y_{\text{best}}}{\sigma(X)} \end{cases}. \quad (12)$$

In Eq. (12), $EI(X)$ is the EI criterion sample set; y_{best} is the current optimal solution; $\hat{y}(X)$ and $\sigma(X)$ are the predicted value and prediction error, respectively; $\Phi(Z)$ and $\phi(Z)$ are the cumulative distribution function and probability density function of the standard normal distribution; Z is the normalized value. The multi-objective optimization process iteratively improves the optimization accuracy, eventually converging to the optimal solution. The convergence condition is shown in Eq. (13).

$$|f_{\text{obj}}^{k+1} - f_{\text{obj}}^k| \leq \epsilon. \quad (13)$$

In Eq. (13), f_{obj}^{k+1} and f_{obj}^k represent the target values for the $k + 1$ -th and k -th optimizations,

This paper has been accepted for publication in the AEE journal. This is the version, which has not been fully edited and content may change prior to final publication.

Citation information: DOI 10.24425/ae.2025.153911

respectively; δ is the convergence threshold. In the THCP-PMSLM motor model, the thermal conduction characteristics of the adiabatic surface, which does not contact air, lead to no heat transfer externally. The adiabatic boundary condition is described in Eq. (14).

$$\lambda_n \frac{\partial T}{\partial n} \Big|_{S_6} = 0. \quad (14)$$

In Eq. (14), λ_n represents thermal conductivity; $\frac{\partial T}{\partial n}$ represents the temperature gradient; S_6 represents the normal direction of the boundary. Thermal conductivity and temperature gradient jointly determine the heat transfer behavior in the material, and the adiabatic boundary condition ensures zero heat transfer at this boundary, resulting in a zero-temperature gradient. These parameter settings ensure the physical accuracy and reasonableness of the model boundary conditions. To ensure that the optimization results meet practical engineering requirements, the optimized parameters are input into COMSOL Multiphysics finite element simulation software to calculate the temperature rise and thrust ripple, as shown in Eq. (15).

$$\begin{cases} \Delta T = f_{\text{FEM}}(X_{\text{opt}}) \\ \Delta F = f_{\text{FEM}}(X_{\text{opt}}) \end{cases} \quad (15)$$

In Eq. (15), ΔT and ΔF represents the temperature rise and thrust ripple; f_{FEM} represents the finite element simulation model; X_{opt} represents the optimized design variables. The cross-section structure and finite element model of the THCP-PMSLM are shown in Fig. 3.

This paper has been accepted for publication in the AEE journal. This is the version, which has not been fully edited and content may change prior to final publication.

Citation information: DOI 10.24425/ae.2025.153911

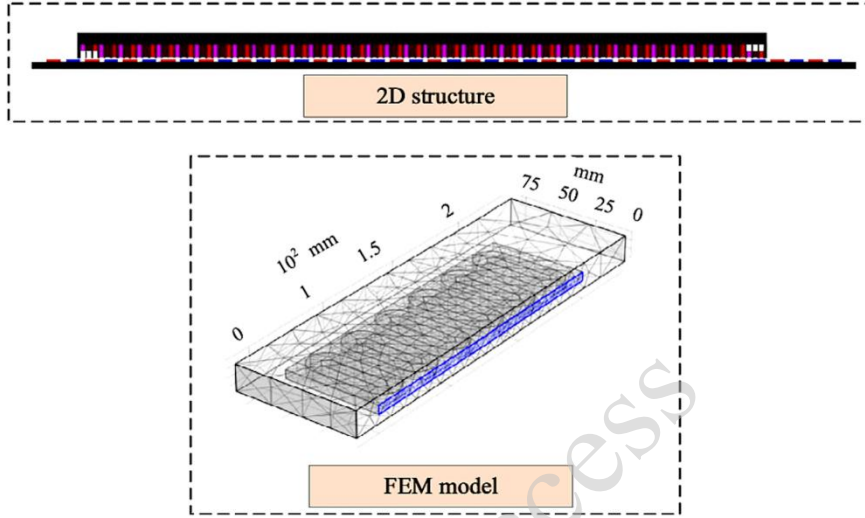


Fig. 3. Cross-section and FEM simulation model of THCP-PMSLM

The 2D cross-section structure of the motor can be seen in Fig. 3, including key components such as stator windings (red and blue parts), permanent magnets (pink parts) and iron core (gray parts). The 2D structure of the motor provides a reference for the finite element modeling of the 3D motor and establishes a finite element mesh to improve the calculation accuracy. Based on the finite element mesh, the magnetic flux of the FEM model is calculated as shown in Eq. (16).

$$\Phi_{\text{total}} = \sum_i B_i \cdot A_i. \quad (16)$$

In Eq. (16), Φ_{total} is the total magnetic flux through a specific region; i denotes the discrete unit index in the finite element model; B_i denotes the magnetic induction at the i -th finite element cell; and A_i denotes the area of the i -th finite element cell.

3. Results

This section evaluates the practical application and performance of the proposed analytical model and optimization method for the PMSLM with a trapezoidal Halbach alternating elec-

This paper has been accepted for publication in the AEE journal. This is the version, which has not been fully edited and content may change prior to final publication.

Citation information: DOI 10.24425/ae.2025.153911

trode structure. A comprehensive evaluation was conducted on temperature field, thrust performance, vibration noise, and economy through COMSOL Multiphysics simulation and Python data analysis.

3.1. Validation and performance evaluation of the PMSLM model with trapezoidal Halbach alternating electrode structure

The proposed method aims to reduce thrust ripple and temperature fluctuations at the same time. To verify the effectiveness of the PMSLM model, it is necessary to define the key specifications of the PMSLM before simulation and experimental testing, as shown in Table 1.

Table 1. Main Specifications of PMSLM

| Parameter | Value/Materials/Winding methods | Unit |
|---------------------------|---------------------------------|------|
| Rated power | 5 | kW |
| Rated voltage | 380 | V |
| Rated current | 15 | A |
| Rated thrust | 200 | N |
| Maximum thrust | 350 | N |
| Rated speed | 2 | m/s |
| Rated efficiency | 92 | % |
| Permanent magnet material | NdFeB | - |
| Coil type | Lap winding | - |
| Pole pitch | 20 | mm |

Based on the above motor parameters, COMSOL Multiphysics 6.0 is used for finite element simulation of the temperature field and thrust performance. The experimental data is processed and visualized using Python 3.9 with the Matplotlib and Pandas libraries. The hardware environment for computations included: Windows 11 operating system, the processor is Intel Core i7-12700H, the clock speed is 2.7 GHz, the memory is 32 GB, and the graphics card is NVIDIA RTX 3060. The experimental platform consisted of a Chroma 62006P-600-8 precision servo power supply and a dynamic motor load testing platform. The Latin hypercube sampling method is used to extract sample points in 3D space and the structural parameters of the sample points are obtained as shown in Fig. 4.

This paper has been accepted for publication in the AEE journal. This is the version, which has not been fully edited and content may change prior to final publication.

Citation information: DOI 10.24425/ae.2025.153911

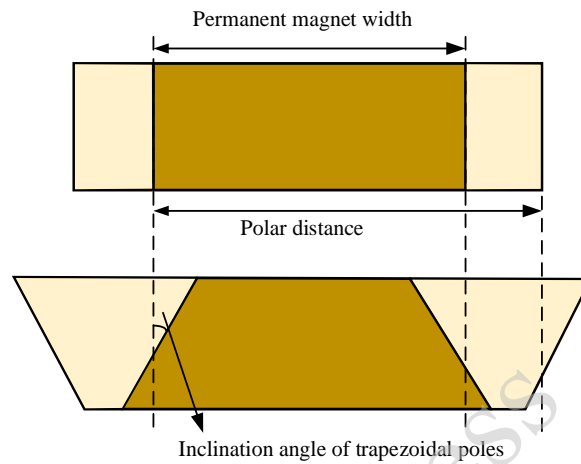


Fig. 4. Schematic diagram of motor structure

Figure 4 shows three structural parameters: pole distance, permanent magnet width and inclination angle of trapezoidal poles. Then, based on these three structural parameters, the average thrust, thrust ripple ratio and thrust per unit volume of the initial sample point are calculated through the ANSYS Maxwell electromagnetic simulation software. The specific contents of the initial sample database are shown in Table 2.

Table 2. Initial sample database

| Permanent magnet width (mm) | Pole distance (mm) | Inclination angle of trapezoidal poles (°) | Average thrust of the linear motor (N) | Thrust ripple ratio (%) | Thrust per unit volume (N/cm ³) |
|-----------------------------|--------------------|--|--|-------------------------|---|
| 14.50 | 18.90 | 24.75 | 44.15 | 36.52 | 2.35 |
| 11.25 | 20.25 | 35.20 | 47.65 | 32.18 | 2.05 |
| 15.18 | 17.75 | 22.40 | 42.80 | 37.85 | 2.35 |
| 12.75 | 19.20 | 33.85 | 49.30 | 29.12 | 2.01 |
| 13.50 | 17.40 | 30.50 | 46.10 | 34.75 | 1.90 |
| ... | ... | ... | ... | ... | ... |
| 10.95 | 18.15 | 40.55 | 65.20 | 16.45 | 2.10 |
| 14.10 | 16.95 | 29.85 | 45.35 | 35.22 | 1.95 |

This paper has been accepted for publication in the AEE journal. This is the version, which has not been fully edited and content may change prior to final publication.

Citation information: DOI 10.24425/ae.2025.153911

To verify the performance of the THCP-PMSLM motor in controlling electromagnetic resistance and generating stable thrust, it was applied in ANSYS Maxwell for electromagnetic simulation and compared with the HCP-PMLSM and the DH-PMLSM. The results are shown in Fig. 5. Figure 5(a) presents the electromagnetic resistance comparison curves. During the motion within the 0–100 mm range, the THCP-PMSLM motor exhibited the smallest fluctuation in electromagnetic resistance, remaining consistently within the range of $[-2, 2]$ N. In contrast, the HCP-PMLSM showed the largest resistance fluctuation, ranging between $[-11, 11]$ N, while the DH-PMLSM had a moderate resistance fluctuation, within the range of $[-5, 5]$ N. Figure 5(b) shows the electromagnetic thrust curves, where the thrust curve of the THCP-PMSLM was the most stable, with a fluctuation range of $[54, 80]$ N. The results demonstrate that the THCP-PMSLM generates more stable thrust with higher accuracy.

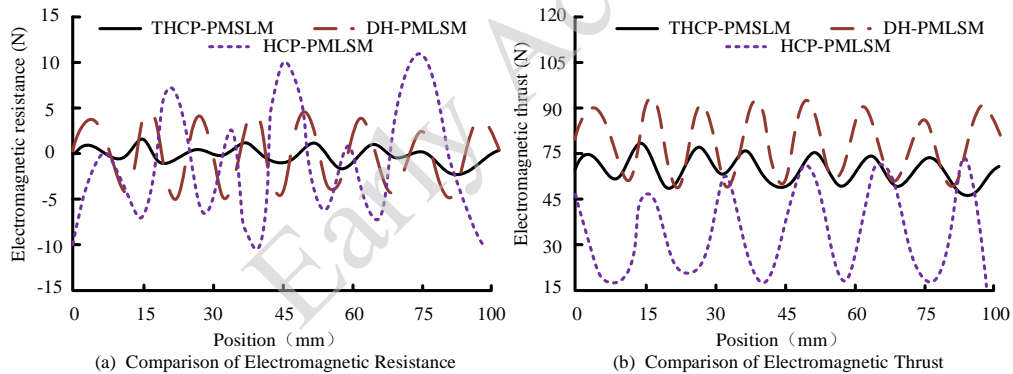


Fig. 5. Comparison of electromagnetic resistance and thrust performance of various models: (a) comparison of electromagnetic resistance; (b) comparison of electromagnetic thrust

To verify the adaptability of the proposed motor under different current excitations, current excitations ranging from 1 A to 7 A were applied. The thrust fluctuation and average thrust of the proposed motor were calculated and compared with those of the HSP-PMLSM and the MRP-PMLSM. Four repeated tests were conducted under the same conditions, and the results are shown in Fig. 6. As seen in Fig. 6(a), the thrust fluctuation of the proposed method stabilized at 8.3%, which was 84.2% and 7.2% lower than that of HSP-PMLSM and MRP-PMLSM, respectively. The average thrust of the proposed method was 69.3 N, 13.2% and 43.4% higher than HSP-PMLSM and MRP-PMLSM, respectively. Overall, in the four repeated tests shown

This paper has been accepted for publication in the AEE journal. This is the version, which has not been fully edited and content may change prior to final publication.

Citation information: DOI 10.24425/ae.2025.153911

in Figs. 6(a), 6(b), 6(c), and 6(d), the quantitative values of thrust fluctuation and average thrust for the three motors exhibited no significant differences, with deviations within 5%. The results indicate that the proposed motor demonstrates high adaptability and stability under different current excitations, making it suitable for practical industrial applications.

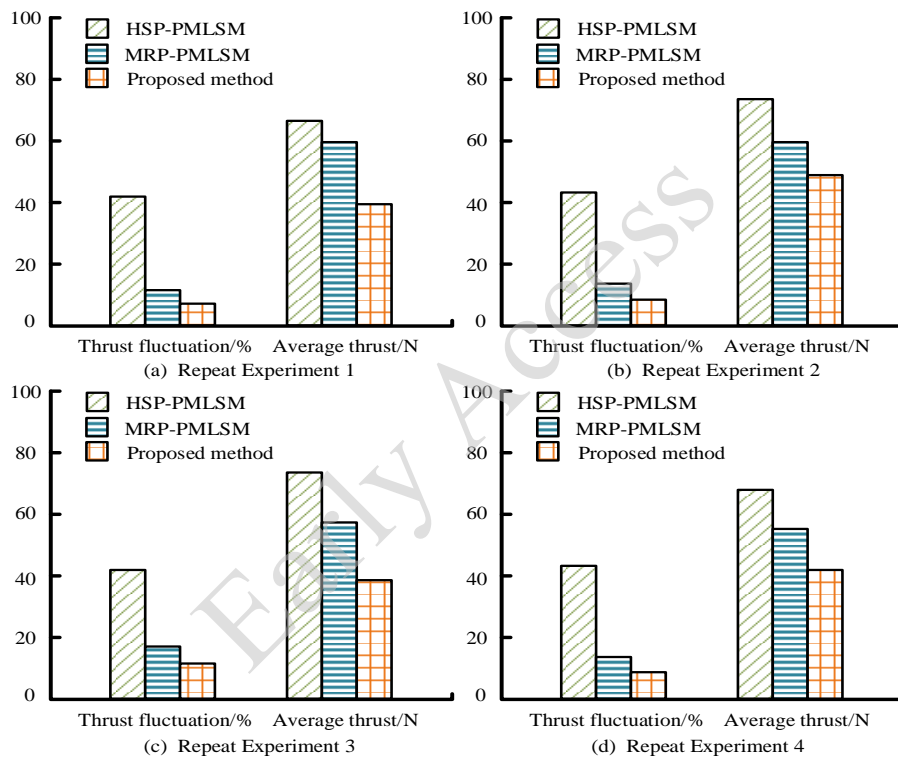


Fig. 6. Comparison of thrust fluctuation and average thrust of each motor: (a) repeat experiment 1; (b) repeat experiment 2; (c) repeat experiment 3; (d) repeat experiment 4

3.2. Analysis of temperature and thrust fluctuation optimization based on the MPGA and Kriging surrogate model.

To validate the effectiveness of the EI criterion and the global search capability of the MPGA, analyzed the co-optimization process of average thrust and thrust fluctuation. The results are illustrated in Fig. 7. As shown in Fig. 7(a), the initial average thrust values were relatively low, primarily ranging from 17 N to 50 N, indicating weak initial design performance. With the optimization process, the added sample points gradually improved the average

This paper has been accepted for publication in the AEE journal. This is the version, which has not been fully edited and content may change prior to final publication.

Citation information: DOI 10.24425/ae.2025.153911

thrust. After 30 iterations, the thrust values stabilized around 70 N. Figure 7(b) highlights the initial large thrust fluctuation, with values ranging from 30% to 65%, reflecting significant instability. The optimized samples demonstrated a steady decline in fluctuation as iterations progressed, eventually reducing to below 10%. These results indicate that the EI criterion significantly enhanced motor thrust performance, stability, and reliability, proving the effectiveness of the optimization method.

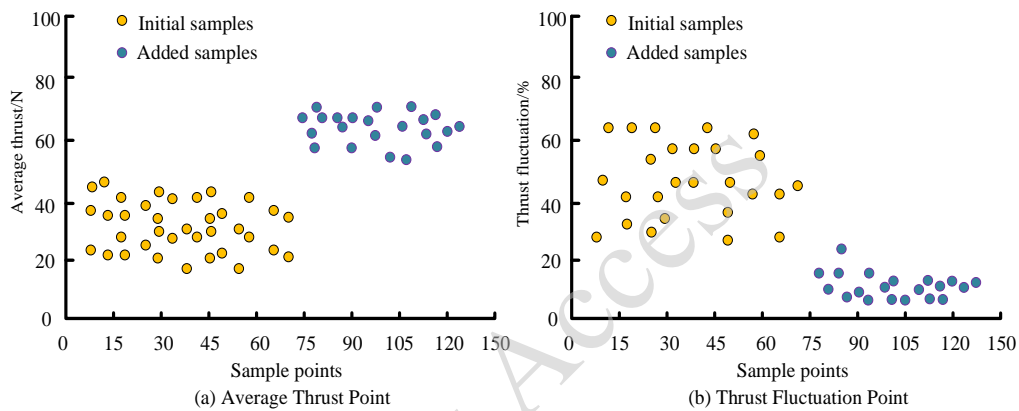


Fig. 7. Data analysis of average thrust and thrust fluctuation point process: (a) average thrust point; (b) thrust fluctuation point

To evaluate the economic performance of the proposed motor, the utilization rate and number of permanent magnets were used as evaluation indicators. Comparisons were made with the VPP-PMLSM and the CCH-PMLSM. The results are shown in Fig. 8. Figure 8(a) demonstrates that as the excitation current increases, the permanent magnet utilization rates of all motors gradually improve. The utilization rate curve of the proposed method remains the highest, reaching a maximum of 5.8 N/cm^3 , which is 3.4% and 27.5% higher than those of the VPP-PMLSM and CCH-PMLSM, respectively. Figure 8(b) shows that the proposed method requires the least amount of permanent magnet material, which is only 0.9 times that of the VPP-PMLSM. The results indicate that the proposed method has optimal economic performance, making it more valuable for application in real industrial environments.

This paper has been accepted for publication in the AEE journal. This is the version, which has not been fully edited and content may change prior to final publication.

Citation information: DOI 10.24425/ae.2025.153911

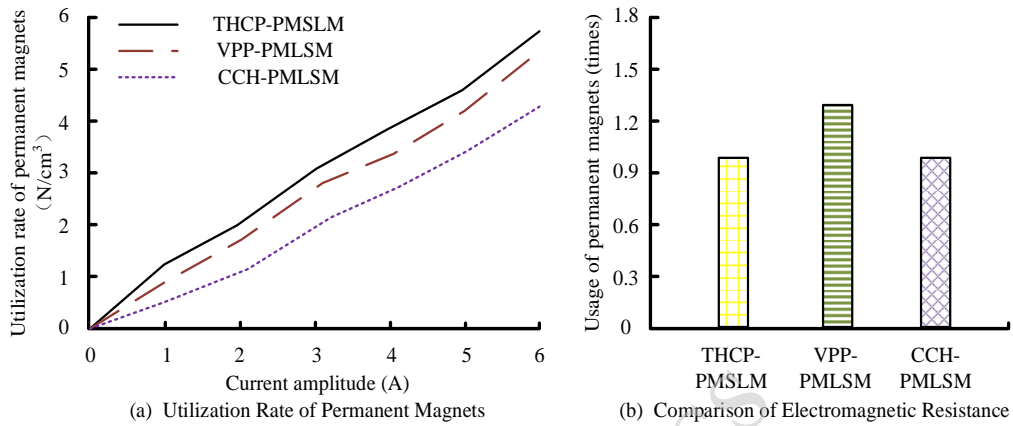


Fig. 8. Economic comparison of various motors: (a) utilization rate of permanent magnets; (b) comparison of electromagnetic resistance

To validate the vibration noise convergence and energy-saving performance of the motor optimized by the proposed MPGA, a comparison was made with two other algorithms designed to solve nonlinear and constrained optimization problems: the DPSO and the AMCO. Figure 9 displays the findings. In Fig. 9(a), it can be observed that as the number of iterations increases, the objective function gradually converges. The proposed algorithm achieves the fastest convergence, reaching 109 dB within 40 iterations. In contrast, DPSO and AMCO converge to 150 dB and 155 dB after 55 and 70 iterations, respectively. Figure 9(b) shows that the proposed method achieves a near 25% energy-saving rate after just 22 iterations, which is 43.5% and 51.3% faster than DPSO and AMCO, respectively. The results demonstrate that the proposed algorithm effectively reduces motor vibration noise while significantly improving energy efficiency.

This paper has been accepted for publication in the AEE journal. This is the version, which has not been fully edited and content may change prior to final publication.

Citation information: DOI 10.24425/ae.2025.153911

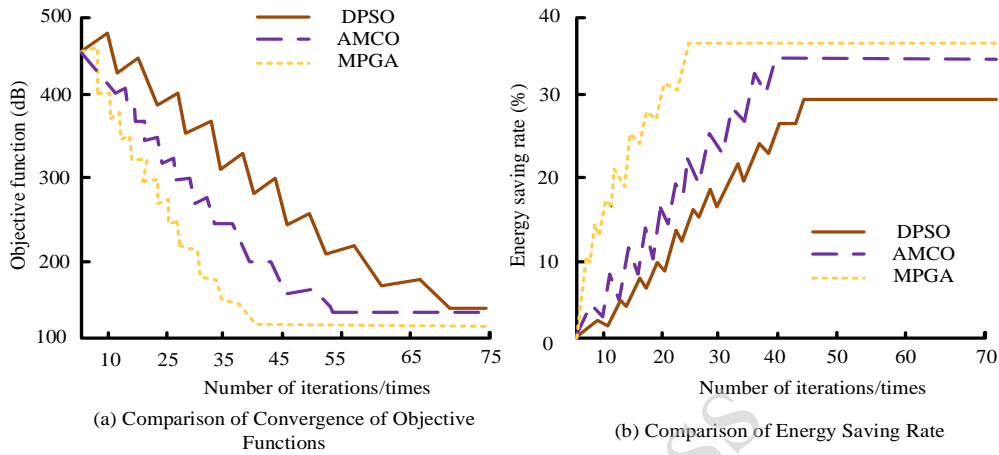


Fig. 9. Comparison of training conditions for various algorithms: (a) comparison of convergence of objective functions; (b) comparison of energy saving rate

To further validate the effectiveness of the proposed analytical model, the data was input into a finite element model for simulation comparison. The magnetic flux was calculated as shown in Eq. (16) and the results are shown in Fig. 10. In Fig. 10(a), at the centerline of the air gap, the radial air gap magnetic flux density waveforms obtained from the finite element simulation and the analytical model overlap, with a difference of only 0.017%. In Fig. 10(b), at the surface of the permanent magnet array, the radial air gap magnetic flux density waveforms from the finite element method also closely match those from the analytical model, with a difference of 0.03%. The consistency between the analytical model and the finite element model is mainly due to the analytical model fully considering the motor's structural parameters, material properties, and boundary conditions during its construction. Additionally, the proposed optimization method helps reduce calculation errors. The results indicate that the proposed method is highly feasible and suitable for practical industrial applications.

This paper has been accepted for publication in the AEE journal. This is the version, which has not been fully edited and content may change prior to final publication.

Citation information: DOI 10.24425/ae.2025.153911

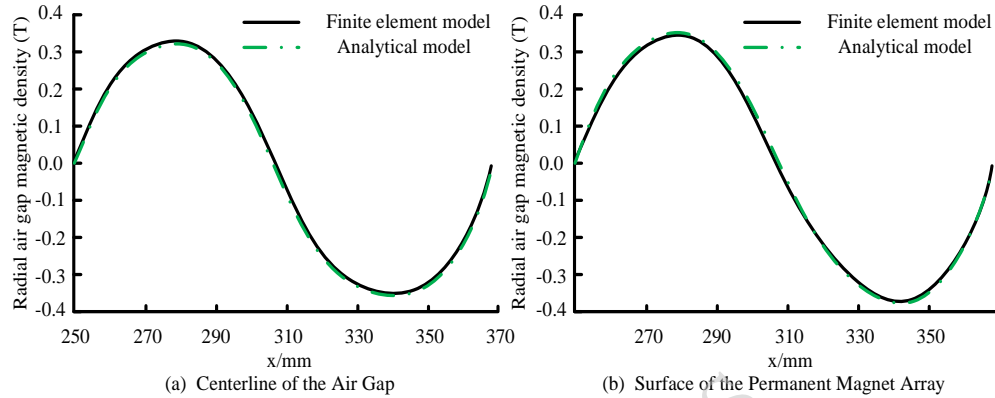


Fig. 10. Analysis of the actual application effect of the model: (a) centerline of the air gap; (b) surface of the permanent magnet array

4. Discussion and conclusion

To address the significant limitations of PMSLMs in thrust fluctuation, electromagnetic noise, and temperature rise control, and to improve the performance stability and adaptability of the PMSLM system, this study proposes an improved method based on electromagnetic structure optimization and temperature-coordinated control. By integrating the THCP-PMSLM model with the MPGA algorithm, significant improvements were achieved in thrust stability, temperature distribution uniformity, and system efficiency. Compared with the Halbach array optimization method, the proposed method introduces a trapezoidal Halbach alternating electrode structure design, significantly reducing thrust fluctuations and enhancing the system's environmental adaptability. When compared with GA-based optimization methods, the study employs an EI criterion and MPGA for multi-objective optimization, achieving faster convergence and higher optimization accuracy. Although some studies have used composite coil optimization strategies to improve motor performance, their high manufacturing cost limits practical application. In contrast, the proposed method demonstrates cost-effective motor performance enhancements, offering significant practical application value. Furthermore, while prior studies utilizing the PSO algorithm for thrust and temperature optimization have suffered from local optima and poor stability, the proposed method effectively overcomes these limitations through improved fitness functions and temperature control strategies.

To tackle these issues, the study introduces an improved method combining novel electro-

This paper has been accepted for publication in the AEE journal. This is the version, which has not been fully edited and content may change prior to final publication.

Citation information: DOI 10.24425/ae.2025.153911

magnetic design and multi-objective optimization algorithms, achieving significant advancements in thrust stability, temperature distribution uniformity, and system efficiency. The proposed method integrates the THCP-PMSLM model with the MPGA algorithm for multi-objective optimization, demonstrating superior performance in both theoretical analysis and experimental validation. Results show that compared with DH-PMLSM and HCP-PMLSM, the proposed method achieves minimal electromagnetic resistance fluctuation, consistently maintained within the range of $[-2, 2]$ N. Its thrust curve is the most stable, with a fluctuation range of $[54, 80]$ N. Thrust fluctuation is stabilized at 8.3%, which is 84.2% and 7.2% lower than the other two motor models, with a variation of less than 5% across four repeated experiments. Optimization reduced thrust fluctuation values from an initial range of 30%–65% to below 10%, while thrust values increased from 17–50 N to approximately 70 N. The proposed method also achieves the highest permanent magnet utilization rate, peaking at 5.8 N/cm^3 , 3.4% and 27.5% higher than VPP-PMLSM and CCH-PMLSM, respectively. Furthermore, it uses the least number of permanent magnets, only 0.9 times that of VPP-PMLSM. The proposed method achieves a maximum energy-saving rate of 25%, converging 43.5% and 51.3% faster than the other two methods. Finite element simulation results highly align with the radial air gap magnetic flux density waveforms of the analytical model. Although the proposed method achieves significant progress in performance optimization, some limitations remain. Its application performance under complex nonlinear conditions can be further optimized in future studies. Enhancing the real-time capabilities and robustness of the algorithm could improve the motor's adaptability to real-world application environments.

Reference

- [1] Wang L., Zhao J., Yang X., Zheng Z., Zhang X., Wang L., *Robust deadbeat predictive current regulation for permanent magnet synchronous linear motor drivers with parallel parameter disturbance and load observer*, IEEE Transactions on Power Electronics, vol. 37, no. 7, pp. 7834–7845 (2022), DOI: [10.1109/tpel.2022.3148389](https://doi.org/10.1109/tpel.2022.3148389).
- [2] Cao M., Nie Z., Song L., Sun J., *GABP-based multiparameter identification for permanent magnet synchronous linear motors*, Journal of Power Electronics, vol. 24, no. 9, pp. 1428–1437 (2024), DOI: [10.1007/s43236-024-00806-4](https://doi.org/10.1007/s43236-024-00806-4).
- [3] Wang C., Yan J., Heng P., Shan L., Zhou X., *Enhanced LADRC for permanent magnet synchronous motor with compensation function observer*, IEEE Journal of Emerging and Selected Topics in Power Electronics, vol. 11, no. 3, pp. 3424–3434 (2023), DOI: [10.1109/JESTPE.2023.3265686](https://doi.org/10.1109/JESTPE.2023.3265686).

This paper has been accepted for publication in the AEE journal. This is the version, which has not been fully edited and content may change prior to final publication.

Citation information: DOI 10.24425/ae.2025.153911

- [4] Zhang Z., Luo M., Duan J., Duan J.A., Kou B., *Design and modeling of a novel permanent magnet width modulation secondary for permanent magnet linear synchronous motor*, IEEE Transactions on Industrial Electronics, vol. 69, no. 3, pp. 2749–2758 (2021), DOI: [10.1109/tie.2021.3065625](https://doi.org/10.1109/tie.2021.3065625).
- [5] Wang L., Zhao J., Zheng Z., *Robust speed tracking control of permanent magnet synchronous linear motor based on a discrete-time sliding mode load thrust observer [J]*, IEEE Transactions on Industry Applications, vol. 58, no. 4, pp. 4758–4767 (2022), DOI: [10.1109/tia.2022.3173594](https://doi.org/10.1109/tia.2022.3173594).
- [6] Wu Q., Wang L., Yang G., Tang E., Wang X., *Ramming mechanism based on permanent magnet synchronous linear motor*, IEEE Transactions on Transportation Electrification, vol. 10, no. 1, pp. 122–134 (2023), DOI: [10.1109/tte.2023.3257922](https://doi.org/10.1109/tte.2023.3257922).
- [7] Li Z., Wang J., An J., Zhang Q., Zhu Y., Liu H., Sun H., *Control strategy of biaxial variable gain cross-coupled permanent magnet synchronous linear motor based on MPC-MRAS*, IEEE Transactions on Industry Applications, vol. 58, no. 4, pp. 4733–4743 (2022), DOI: [10.1109/tia.2022.3170535](https://doi.org/10.1109/tia.2022.3170535).
- [8] Zhang Z., Luo M., Duan J., Kou B., *Design and analysis of a novel frequency modulation secondary for high-speed permanent magnet linear synchronous motor*, IEEE/ASME Transactions on Mechatronics, vol. 27, no. 2, pp. 790–799 (2021), DOI: [10.1109/tmech.2021.3071549](https://doi.org/10.1109/tmech.2021.3071549).
- [9] Di J., Fletcher J.E., Li W., *Simplified piecewise model of line-start permanent magnet linear synchronous motors*, IEEE Transactions on Industry Applications, vol. 58, no. 5, pp. 6093–6104 (2022), DOI: [10.1109/tia.2022.3183558](https://doi.org/10.1109/tia.2022.3183558).
- [10] Yang X., Yang R., Tan S., Yu X., Fang L., *MPGA-based-ECMS for energy optimization of a hybrid electric city bus with dual planetary gear*, Proceedings of the Institution of Mechanical Engineers, Part D: Journal of Automobile Engineering, vol. 236, no. 8, pp. 1889–1909 (2022), DOI: [10.1177/09544070211041074](https://doi.org/10.1177/09544070211041074).
- [11] Yun H., Bu Z., Yang Z., Wang L., Zhang B., *Optimization of fuel injection timing and ignition timing of hydrogen fueled SI engine based on DOE-MPGA*, International Journal of Hydrogen Energy, vol. 48, no. 25, pp. 9462–9473 (2023), DOI: [10.1016/j.ijhydene.2022.12.068](https://doi.org/10.1016/j.ijhydene.2022.12.068).
- [12] Chen Y., Cui C., Wu Y., *Nondestructive detection model of soluble solids content of an apple using visible/near-infrared spectroscopy combined with CARS and MPGA*, Applied Optics, vol. 60, no. 27, pp. 8400–8407 (2021), DOI: [10.1364/ao.439291](https://doi.org/10.1364/ao.439291).
- [13] Wu Y.Z., Fan Y.R., Wu Z.G., Deng S., Zhang P., Chen S., Yin Z., *A fast inversion method for array laterolog based on convolutional neural network and hybrid MPGA-LM algorithm*, Chinese Journal of Geophysics, vol. 64, no. 9, pp. 3410–3425 (2021), DOI: [10.6038/cjg202100499](https://doi.org/10.6038/cjg202100499).
- [14] Zhang S., Qiang J., Liu H., Wang X., Zhou J., Fan D., *An adaptive dynamic kriging surrogate model for application to the optimal remediation of contaminated groundwater*, Water Resources Management, vol. 36, no. 13, pp. 5011–5032 (2022), DOI: [10.1007/s11269-022-03289-9](https://doi.org/10.1007/s11269-022-03289-9).
- [15] Zhang S., Qiang J., Liu H., Zhu X., Lv H., *A construction strategy for conservative adaptive*

This paper has been accepted for publication in the AEE journal. This is the version, which has not been fully edited and content may change prior to final publication.

Citation information: DOI 10.24425/ae.2025.153911

Kriging surrogate model with application in the optimal design of contaminated groundwater extraction-treatment, Environmental Science and Pollution Research, vol. 29, no. 28, pp. 42792–42808 (2022), DOI: [10.1007/s11356-021-18216-5](https://doi.org/10.1007/s11356-021-18216-5).

- [16] Huang M., Leung V.C.M., Liu A., Xiong N.N., *TMA-DPSO: Towards efficient multi-task allocation with time constraints for next generation multiple access*, IEEE Journal on Selected Areas in Communications, vol. 40, no. 5, pp. 1652–1666 (2022), DOI: [10.1109/jsac.2022.3143205](https://doi.org/10.1109/jsac.2022.3143205).
- [17] Mahmood D.Y., Abd M.K., Jalal K.A., *Wind Energy Output Prediction Model Based on DPSO-BP Neural Network*, International Journal of Intelligent Engineering & Systems, vol. 14, no. 1, pp. 242–254 (2021), DOI: [10.22266/ijies2021.0630.21](https://doi.org/10.22266/ijies2021.0630.21).
- [18] Kwon J.H., Kim J.K., Jeon E.S., *Shape Optimization of PMLSM Stator for Reduce Thrust Ripple Components Using DOE*, Journal of the Semiconductor & Display Technology, vol. 20, no. 4, pp. 38–43 (2021), DOI: [10.3390/app112211066](https://doi.org/10.3390/app112211066).
- [19] Shiliang Y., Wang Y., Lu D., Pan X., *Simulation and Optimization of Permanent Magnet Linear Machine Based on Deep Neural Network*, Journal of System Simulation, vol. 36, no. 3, pp. 713–725 (2024), DOI: [10.16182/j.issn1004731x.joss.23-0211](https://doi.org/10.16182/j.issn1004731x.joss.23-0211).
- [20] Liu C., Yao J., Jia Y., *Vehicle height control based on active suspension with permanent magnet synchronous linear motor*, Proceedings of the Institution of Mechanical Engineers, Part D: Journal of Automobile Engineering, vol. 238, no. 5, pp. 1191–1200 (2024), DOI: [10.1177/0954407022114149](https://doi.org/10.1177/0954407022114149).
- [21] Ni Y., Qiu Z., Xiao B., *Investigation of surface-inset Halbach machines with trapezoidal mixed grade magnets*, International Journal of Applied Electromagnetics and Mechanics, vol. 72, no. 4, pp. 387–408 (2023), DOI: [10.3233/JAE-220192](https://doi.org/10.3233/JAE-220192).
- [22] Zeng R., Zhao J., Yan S., Mao Y., *Research on cogging force suppression for toroidal pmlsm based on disturbance observer*, CES Transactions on Electrical Machines and Systems, vol. 7, no. 2, pp. 187–192 (2023), DOI: [10.30941/CESTEMS.2023.00017](https://doi.org/10.30941/CESTEMS.2023.00017).
- [23] Li Z., Zhang Z.H., Wang J.S., Yan Z.B., Guo X.Q., Sun H.X., *Nonsingular Fast Terminal Sliding Mode Control Strategy for PMLSM Based on Disturbance Compensation*, Journal of Electrical Engineering & Technology, vol. 19, no. 3, pp. 1331–1342 (2024), DOI: [10.1007/s42835-023-01590-0](https://doi.org/10.1007/s42835-023-01590-0).
- [24] Sohail A., *Genetic algorithms in the fields of artificial intelligence and data sciences*, Annals of Data Science, vol. 10, no. 4, pp. 1007–1018 (2023), DOI: [10.1007/s40745-021-00354-9](https://doi.org/10.1007/s40745-021-00354-9).
- [25] Hamdia K.M., Zhuang X., Rabczuk T., *An efficient optimization approach for designing machine learning models based on genetic algorithm*, Neural Computing and Applications, vol. 33, no. 6, pp. 1923–1933 (2021), DOI: [10.1007/s00521-020-05035-x](https://doi.org/10.1007/s00521-020-05035-x).
- [26] Nikbakht S., Anitescu C., Rabczuk T., *Optimizing the neural network hyperparameters utilizing genetic algorithm*, Journal of Zhejiang University-Science A, vol. 22, no. 6, pp. 407–426 (2021), DOI: [10.1631/jzus.a2000384](https://doi.org/10.1631/jzus.a2000384).

This paper has been accepted for publication in the AEE journal. This is the version, which has not been fully edited and content may change prior to final publication.

Citation information: DOI 10.24425/ae.2025.153911

- [27] Garud K.S., Jayaraj S., Lee M.Y., *A review on modeling of solar photovoltaic systems using artificial neural networks, fuzzy logic, genetic algorithm and hybrid models*, International Journal of Energy Research, vol. 45, no. 1, pp. 6–35 (2021), DOI: [10.1002/er.5608](https://doi.org/10.1002/er.5608).
- [28] Velliangiri S., Karthikeyan P., Xavier V.M.A., Baswaraj D., *Hybrid electro search with genetic algorithm for task scheduling in cloud computing*, Ain Shams Engineering Journal, vol. 12, no. 1, pp. 631–639 (2021), DOI: [10.1016/j.asej.2020.07.003](https://doi.org/10.1016/j.asej.2020.07.003).
- [29] Palanisamy R., Govindaraj V., Siddhan S., Albert J.R., *Experimental investigation and comparative harmonic optimization of AMLI incorporate modified genetic algorithm using for power quality improvement*, Journal of Intelligent & Fuzzy Systems, vol. 43, no. 1, pp. 1163–1176 (2022), DOI: [10.3233/jifs-212668](https://doi.org/10.3233/jifs-212668).
- [30] Dang X., Gong D., Yao X., Tian T., Liu H., *Enhancement of mutation testing via fuzzy clustering and multi-population genetic algorithm*, IEEE Transactions on Software Engineering, vol. 48, no. 6, pp. 2141–2156 (2021), DOI: [10.1109/TSE.2021.3052987](https://doi.org/10.1109/TSE.2021.3052987).
- [31] Yu W., Yang G., Wang L., Lin D., Al-Zahrani A., *Improved flux linkage observer for position estimation of permanent magnet synchronous linear motor*, Mechanical Sciences, vol. 15, no. 1, pp. 99–109 (2024), DOI: [10.5194/ms-15-99-2024](https://doi.org/10.5194/ms-15-99-2024).
- [32] Li Z., Wu L., Li Y., Lu Q., Huang X., Peretti L., Shen Y., *Hybrid analytical model of permanent magnet linear motor considering iron saturation and end effect*, IEEE transactions on energy conversion, vol. 39, no. 3, pp. 2008–2017 (2024), DOI: [10.1109/TEC.2024.3354488](https://doi.org/10.1109/TEC.2024.3354488).